Field- and photofield-emission spectroscopy of sodium overlayers on the (100) and (110) facets of tungsten

A. Derraa
Department of Physics, University of Toronto, Toronto, Ontario, Canada M5S 1A7

M. J. G. Lee
Department of Physics and Scarborough College, University of Toronto, Toronto, Ontario, Canada M5S 1A7
(Received 26 March 1998; revised manuscript received 9 November 1998)

Sodium overlayers on the (100) and (110) facets of a tungsten field emitter in the range of coverage from 0 to 1.2 monolayers have been studied by means of field- and photofield-emission spectroscopy. On the (100) facet, the adatom configuration is strongly influenced by the applied electric field. On the (110) facet, a planar island of sodium grows on top of the first monolayer. The observed energy dependencies of the surface densities of states of Na/W(100) and Na/W(110) show similar features that are related to the valence electronic levels of sodium weakly perturbed by interaction with the substrate. The data provide evidence that a sodium monolayer strongly enhances field emission from below the Fermi level on W(100) but not on W(110). [S0163-1829(99)09315-7]

I. INTRODUCTION

Alkali-metal atoms adsorbed on metallic substrates have been investigated over many years, and are widely regarded as being among the simplest of adsorbate systems. Absorption phenomena continue to be an active area of research because of various unsettled fundamental issues.[1] Among these are questions about the adatom-metal interaction, including the bonding character at submonolayer coverage and the electronic structure of the interface. Recent experimental findings have called into question the physically appealing model of Gurney,[2] which postulated an ionic-to-metallic change with increasing adsorbate coverage. Woratschek *et al.*[3] have reported that emission from atomic *s* levels can be detected in the K/Cu(110) system at a coverage of 0.02 monolayer (ML), indicating that adsorbed potassium has significant nonionic character even at very low coverage. However, Lee *et al.*[4] have interpreted an analogous structure in the K/Ni(111) system as involving the electronic states of the substrate.

The presence of adsorbates at a metal-vacuum interface modifies the electronic structure of the interface. An investigation of the electronic structure of a metal-adsorbate-vacuum interface requires a highly surface-sensitive experimental technique. Photofield emission, measured in conjunction with field emission, can be used to probe the electronic states of the interface that lie between the Fermi level and the vacuum level. The sample is illuminated by a focused *p*-polarized laser beam with a photon energy smaller than the work function, and a strong static electric field is applied at the metal-vacuum interface. Singly photoexcited electrons escape from the metal either by tunneling through the surface potential barrier or by passing above it. Features in the total-energy distribution of the emitted electrons yield information about the electronic structure of the interface in the vicinity of E_F, while their dependencies on the photon energy make it possible to distinguish unambiguously between initial- and final-state structures.

The present paper reports the results of an experimental investigation of sodium adsorbed on W(100) and W(110) at room temperature by means of field- and photofield-emission spectroscopy in the range of exposure from 0 to 1.2 ML. Below 1 ML exposure, sodium adatoms are found to bond more strongly to the (100) facet than to the (110) facet, and above 1 ML exposure, two-dimensional island formation occurs on W(110) but not on W(100). The data are interpreted by comparing them with the results of electronic structure calculations for sodium singly adsorbed on jellium. It is concluded that the observed sodium-induced features in the surface electronic densities of states, which are similar on the two planes, are related to the valence electronic levels of sodium weakly perturbed by interaction with the substrate. A comparison between the present data and the results of a full-potential linearized-augmented-plane-wave calculation of the electronic structure of the tungsten-sodium-vacuum interface will be reported elsewhere.

The remainder of this paper is organized as follows. Section II provides a brief description of the experimental apparatus and the method of data analysis. The experimental results are presented in Sec. III and discussed in Sec. IV. Section V is a summary of the results and conclusions of the present work.

II. EXPERIMENT

A. Apparatus and experimental procedure

The field- and photofield-emission spectrometer has been described in detail elsewhere.[5] The experimental chamber contains the field emitter and the energy analyzer, and the deposition chamber contains the Knudsen cell that serves as the atomic beam source. The experimental chamber and the deposition chamber are independently pumped and interconnected by a duct fitted with a gate valve. A 1-mm-diam aperture restricts the flow of gas between the two chambers during deposition, thereby minimizing contamination of the

tip due to outgassing by the Knudsen cell. With this arrangement, the base pressure in the experimental chamber remains below 10^{-10} torr even when, during deposition, the pressure in the deposition chamber rises to 10^{-8} torr. Quartz ampoules were filled with 99.9% pure sodium and sealed under argon. A sealed ampoule was inserted into the Knudsen cell, and the neck of the ampoule was broken under vacuum by flexing it with an externally controlled mechanical lever. The sodium source was outgassed at 100 °C for about three days, then for a few hours at 200 °C. To deposit sodium on the field emitter, the Knudsen cell was heated to 250 °C.

In the experimental chamber, a tungsten field emitter is mounted on a sample holder about 5 cm from a fluorescent conducting screen. The tip is grounded, and the potential difference between the tip and the screen is maintained at several kilovolts. The beam of electrons emitted from a single facet is selected by electrostatically deflecting the field-emission pattern so that the image of the desired facet is centered over a small probe hole in the middle of the fluorescent screen. Electrons that pass through the probe hole enter a double-pass cylindrical energy analyzer, and electrons within the selected energy range are detected by means of a spiraltron electron multiplier. The laser illumination system used for photofield-emission measurements is mounted outside the vacuum chamber. The apparatus is controlled by means of a PC-based data acquisition system.

Prior to deposition the field emitter was carefully aligned with the Knudsen cell and the collimating aperture, then cleaned by flashing to incandescence. Both Fowler-Nordheim (FN) data (measurements of the total-emission current from a single facet as a function of the tip-to-screen potential difference) and total-energy distribution (TED) data (measurements of the emission current from a single facet in a narrow energy range as a function of total electron energy) for the clean facet were recorded. The flux of sodium atoms was measured by means of a quartz crystal monitor mounted at right angles to the direction of the atomic beam, and the exposure was calculated from the dimensions of the apparatus and the angle of incidence onto the emitting facet. To estimate the coverage from the exposure, a sticking coefficient of unity was assumed.[6] Sodium atoms were deposited at very low flux (typically 0.1 ML/min) onto the selected facet {(100) or (110)}. During deposition, the potential difference between the tip and the screen was held constant, and both the field-emission pattern and the emission current from the center of the facet were monitored continuously. Once the desired coverage had been reached, total-energy distributions in field emission and in photofield emission were recorded. The tip bias voltage was stepped through 100 channels, each of width 25 mV, spanning the appropriate energy range, the tip-to-screen potential difference being held constant. At each step the bias voltage was allowed to stabilize for 10 μs, then the detected electrons were counted for 500 μs. The sweep sequence was repeated, typically for 1000 cycles in field emission and for 2000 cycles in photofield emission, until adequate statistics had been achieved. For measurements of photofield emission the tip was illuminated by a focused *p*-polarized laser beam at a large angle of incidence in order to enhance surface photoexcitation.[7] All of the measurements were carried out at room temperature. Once all of the measurements at a given adsorbate coverage were complete, the tip was repeatedly flashed to remove the sodium overlayer, and sodium was deposited to the next exposure. The very high reproducibility of the dependence of the total-emission current on deposition time demonstrated that the sodium flux was very stable throughout the experiment.

B. Data analysis

According to the free-electron model, the total-energy distribution in field emission, $j_0(E)$, is given by[11,12]

$$j_0(E)=(em/2\pi^2\hbar^3)f(E)\int_{-V_0}^{E}D(W)dW, \tag{1}$$

where $f(E)$ is the Fermi-Dirac distribution function, $D(W)$ is the probability of transmission through the surface potential barrier, W is the normal energy of the field-emitted electrons, and $-V_0$ is the energy of the bottom of the conduction band. If the transmission probability is evaluated in the WKB approximation,[8] Eq. (1) can be expressed approximately in the form

$$j_0(E)=A\exp[(E-E_F)/d]\{1+\exp[-(E-E_F)/kT]\}^{-1}, \tag{2}$$

where A is a constant, E is the total energy of the emitted electron, E_F is the Fermi energy, and $d\propto F/\phi^{1/2}$, where ϕ is the work function and F is the strength of the applied electric field. The total-energy distribution $j_0(E)$ decreases exponentially both below E_F, due to the increasing thickness of the surface potential barrier, and above E_F, due to the decreasing probability of occupation of electronic states as described by the Fermi-Dirac distribution function. It follows from Eq. (2) that, in the free-electron approximation, a plot of $\ln j_0(E)$ against E at $T=0$ will be triangular in form with a peak at $E=E_F$. At finite temperatures the energy of the peak is unchanged, but a slight rounding of the peak is predicted.

Features in the electronic structure of a real metal-adsorbate-vacuum interface are expected to show up as deviations of the plot from the ideal triangular form. Therefore, information about the surface density of electronic states at a metal-adsorbate-vacuum interface can be extracted by comparing the experimental total-energy distribution $j(E)$ with the calculated free-electron distribution $j_0(E)$. It is convenient to express the measured distribution $j(E)$ in the form of the enhancement factor $R(E)$, which is defined by

$$R(E)=j(E)/[j_0(E)\otimes\Delta(E)], \tag{3}$$

where the free-electron distribution $j_0(E)$ is convolved with a Gaussian instrumental resolution function $\Delta(E)$ that represents the finite resolution of the energy analyzer.[9] Modinos has shown that the enhancement factor defined this way is closely related to the electronic density of states in the surface layer.[10]

The free-electron distribution $j_0(E)$ was calculated numerically from Eq. (1) using transmission probabilities derived from an exact numerical solution of the Schrödinger equation for the image potential barrier.[11] The enhancement factor involves an undetermined normalizing constant because neither the area of the emitting surface that is sampled by the probe hole nor the collection efficiency of the energy analyzer was determined in the present work. The effect of

this normalizing constant can be removed by plotting $\ln R$ as a function of energy. The enhancement factors are useful for emphasizing small deviations from free-electron theory, but in the presence of sodium overlayers on tungsten the deviations from free-electron theory are typically so large that it is more meaningful to plot the experimental total-energy distributions. In the present paper the enhancement factors are also reported in a few cases where this serves to emphasize significant features of the experimental distributions.

According to the free-electron model, the total-energy distribution in photofield emission is given by[12]

$$j_0^{\mathrm{PFE}}(E)=Nf(E-\hbar\omega)\int_{-V_0}^{E-\hbar\omega}[(W+V_0)\times(W+\hbar\omega+V_0)]^{-1/2}|M|^2D(W+\hbar\omega)dW, \tag{4}$$

where M is the matrix element that governs the photon-induced transition between the initial state of energy $E-\hbar\omega$ and the final state of energy E, $D(W)$ is the probability of transmission through the surface potential barrier, and N is a constant factor. W is the normal energy of the initial state measured relative to the bottom of the conduction band, and $f(E-\hbar\omega)$ is the Fermi-Dirac distribution that governs the probability of occupation of the initial state. Equation (4) was evaluated numerically by assuming that $|M|^2$ is independent of W for initial and final states separated by one photon energy.[13] In this approximation $|M|^2$ can be taken outside the integral, and then $j_0^{\mathrm{PFE}}(E)$ can be evaluated as for field emission. In the free-electron approximation, the shape of the total-energy distribution in photofield emission is similar to that in field emission except that the peak occurs at $E_F+\hbar\omega$, where $\hbar\omega$ is the photon energy. For reasons to be discussed in Sec. III, it proved to be impossible to measure the work function in the present experiment. The work function data used to compute the enhancement factor were taken from the work of Klimenko and Medvedev.[14]

III. RESULTS

A. Field-emission pattern

Figures 1(a)–1(d) show the evolution of the field-emission pattern as a function of sodium exposure on the (110) facet of a tungsten field emitter at room temperature. The exposures are expressed in monolayers [1 ML corresponds to a (2×2)Na-W(110) structure]. A field-emission pattern of similar appearance is observed when the sodium flux is incident on the W(100) facet. Below 1 ML exposure the pattern is similar to that of a clean tip, but with increasing exposure the high-index regions become brighter and the size of the (110) plane increases noticeably relative to that of the clean tip. Above 1 ML exposure, a bright ringlike feature appears in the center of the (110) plane. Initially, the edges of this feature are brighter than its center but with increasing coverage it is transformed to an island of uniform brightness at 1.5 ML. The size of this island remains constant until the second monolayer is complete. At 2 ML exposure the W(110) plane becomes uniformly bright.

If the flux of sodium is interrupted just above 1 ML exposure, the island disappears over a time interval of a few minutes, presumably because sodium atoms diffuse to the surrounding facets. If the plane is once again exposed to the sodium flux, an island identical to that observed in the initial deposit immediately reappears. If the sodium flux is stopped above 1.5 ML, the island is fairly stable at room temperature, but increasing the tip temperature to above 200 °C causes the island to shrink and eventually to disappear. At 2 ML exposure the whole pattern becomes uniformly bright, and none of the characteristic features of the field-emission pattern of clean tungsten remain. Moderate heating (to 400 °C) makes the field-emission pattern go through these various stages in reverse order, showing that sodium adatoms are easily removed from the tip by evaporation. Neither the strength of the applied electric field nor the deposition rate has any appreciable effect on the appearance of the island. It is interesting to note that identical stages of island growth are observed when the W(110) plane is not directly exposed to the sodium flux. In this case, the growth of the island presumably involves surface migration.

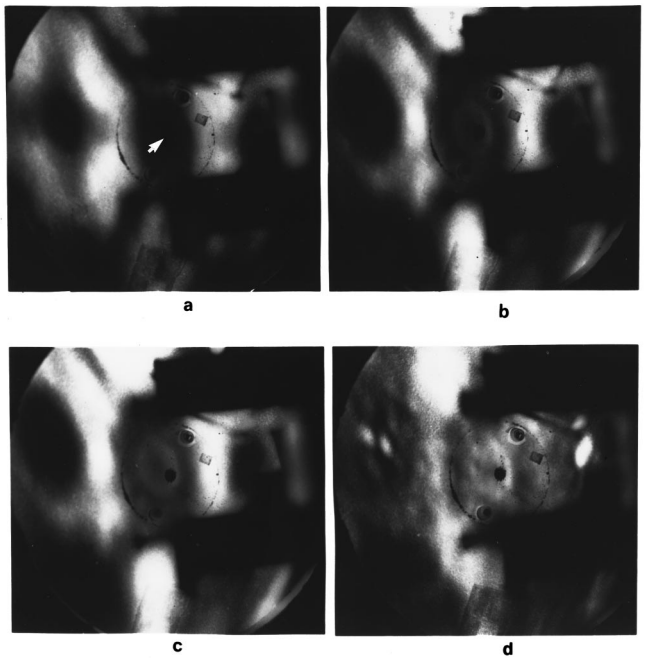

FIG. 1. Evolution of the field-emission pattern as a function of sodium exposure on W(110). (a) 0.8 ML, (b) 1.2 ML, (c) 1.5 ML, (d) 2.0 ML. The white arrow in (a) indicates the (110) facet. The dark patches to left and right of the (110) facet are the (100) facets, and the bright patches above and below the (110) facet are the (111) facets. The additional objects visible around the probe hole are supports for the screen.

B. Total-emission current and total-energy distributions from Na/W(100)

Figure 2 is a plot of the total field-emission current from W(100) measured as a function of sodium exposure with a constant potential difference applied between the tip and the screen. Initially the emission current increases slowly with increasing exposure. It passes through a weak maximum near 1 ML, decreases, and then increases rapidly. As the exposure approaches 1 ML, random spikes are observed in the emission current. Fluctuating bright spots observed in the field-

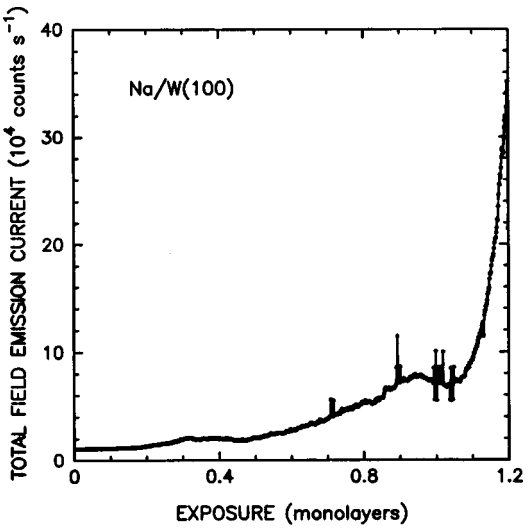

FIG. 2. The total field-emission current from the center of the W(100) facet at 300 K, plotted as a function of sodium exposure.

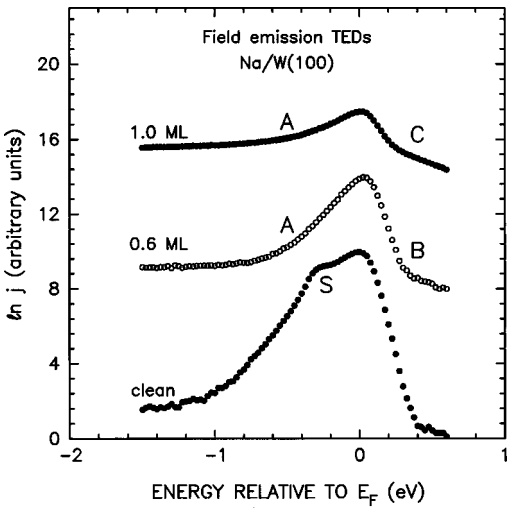

FIG. 3. Representative field-emission total-energy distributions for emission from the (100) facet of tungsten at room temperature, for a series of sodium exposures. The extended low- and high-energy tails (labeled *A* and *C*) are discussed in the text. The prominent features in the clean distribution 0.35 eV below E_F is the Swanson peak (labeled *S*). The curves have been displaced vertically for clarity.

emission pattern suggest that these spikes correspond to the formation of small transient atomic clusters within the region of the emitting facet that is sampled by the probe hole.

In the conditions of the present experiment, sodium adatoms on W(100) are strongly influenced by the applied electric field. After the sodium flux was stopped, repeatedly switching the field off and on caused random changes in the field-emission pattern and in the emission current due to the migration of sodium atoms across the emitting facet. The changes occurred so rapidly that it was not possible to record them with the present apparatus; video photography might make it possible to follow the motion of the adsorbate. When the field was switched off, the total-emission current fell to zero. When the field was switched back on, the emission current was typically much larger than before, but it decayed rapidly to close to its initial value. The transient increase in the emission current when the field was switched off and on again grew with increasing exposure. Above 2 ML exposure this field effect disappeared completely, and neither the field-emission pattern nor the total field-emission current was sensitive to the strength of the electric field at the emitting surface.

Representative field-emission total-energy distributions for Na/W(100) in the range of exposure from 0 to 1.0 ML are shown in Fig. 3. The bottom curve is the spectrum of the clean W(100) plane, showing the Swanson peak (labeled *S*) 0.35 eV below the Fermi level. Above 0.6 ML the Swanson peak is completely quenched, and by 1.0 ML extended low-energy (labeled *A*) and high-energy (labeled *C*) tails appear in the TED.

Experimental photofield-emission TEDs for photon energies of 2.604 and 3.049 eV are shown in Figs. 4 and 5, respectively. The greater noise in the 2.604-eV curves is attributable to the low power in the laser beam at this photon energy. Above 0.5 ML the TEDs at 2.604 eV show a hump (labeled *B* in Fig. 4) centered about 2.4 eV above E_F, while the TEDs at 3.049 eV show a broad peak (labeled *B* in Fig. 5) centered about 2.2 eV above E_F. The similar appearances and energies of these structures suggest that they are due to a final-state resonance. These structures broaden asymmetrically to lower energy with increasing exposure, and the TEDs show prominent low- and high-energy tails at an exposure of 1 ML.

C. Total-emission current and total-energy distributions for Na/W(110)

Figure 6 is a plot of the total field-emission current from W(110), measured as a function of the sodium exposure, with a constant potential difference applied between the tip and the screen. Below 1 ML the smooth variation of the

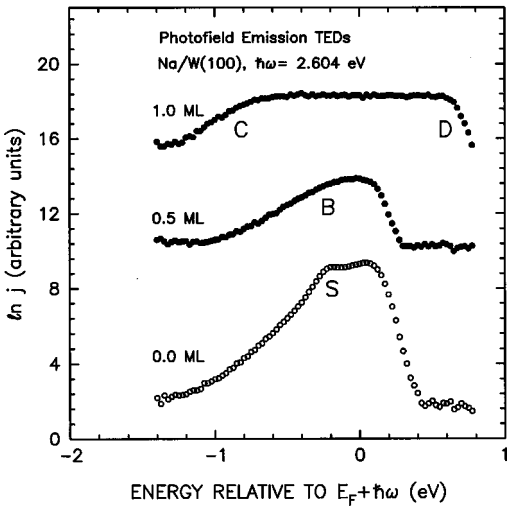

FIG. 4. Representative photofield-emission total-energy distributions ($\hbar\omega = 2.604$ eV) for emission from the (100) facet of tungsten at room temperature, for a series of sodium exposures. *B*, *C*, and *D* denote features of the distributions that are discussed in the text. The prominent peak in the clean distribution 0.35 eV below E_F is the Swanson peak (labeled *S*). The curves have been displaced vertically for clarity.

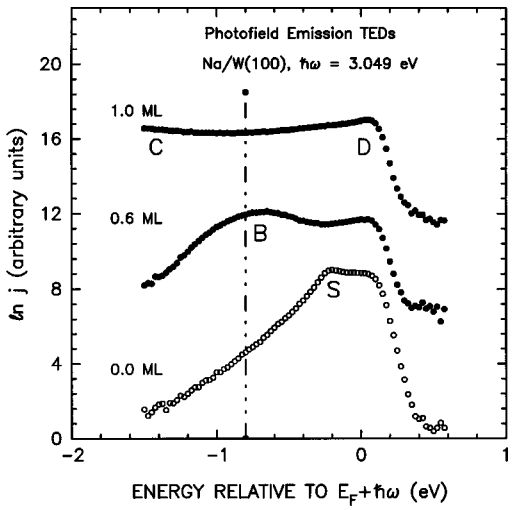

FIG. 5. Representative photofield-emission total-energy distributions ($\hbar\omega = 3.049$ eV) for a series of sodium exposures on the (100) facet of tungsten at room temperature. *B*, *C*, and *D* denote features of the distributions that are discussed in the text. The peak in the clean distribution 0.35 eV below E_F is the Swanson peak (labeled *S*). The curves have been displaced vertically for clarity.

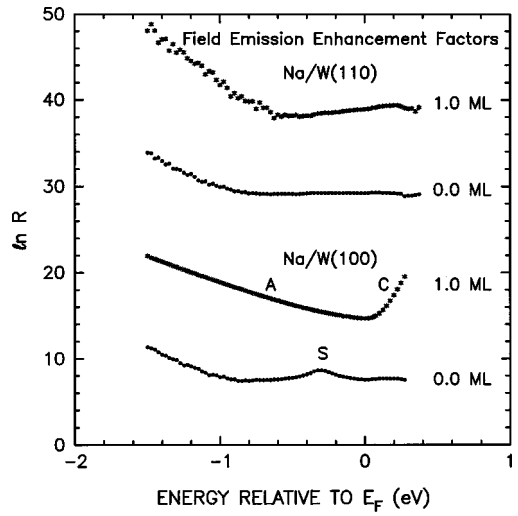

FIG. 7. Comparison between the enhancement factors for field emission from the (100) and (110) facets of tungsten at room temperature for sodium exposures of 0 and 1 ML. 1 ML of sodium induces strong departures from free-electron behavior (*A*,*C*) on (100) but not on (110). *S* denotes the Swanson peak. The tails in the enhancement factors below about −0.8 eV are due to electron scattering in the energy analyzer.

total-emission current with increasing exposure shows that the adsorbate is uniformly distributed on the substrate. The abrupt increase in the total field-emission current that occurs at 1 ML coincides with the appearance of an island in the field-emission pattern. Above 1 ML, large fluctuations in the total-emission current and fluctuating bright spots in the field-emission pattern indicate the formation of transient clusters. If the sodium flux is stopped just above 1 ML, the total field-emission current relaxes back to close to its value at 1 ML, but if the flux is stopped above 1.5 ML the current does not relax back at all.

The enhancement factors plotted in Fig. 7 show that the field-emission TEDs for Na/W(110) are featureless over the range of exposure from 0 to 1.0 ML. Unlike Na/W(100), there is no indication of an adsorbate-induced low-energy tail in the field-emission TED. The corresponding photofield-emission data at a photon energy of 3.049 eV are featureless below 0.5 ML exposure, but those at 0.6 ML show a sodium-induced peak (labeled B' in Fig. 8) centered at about 0.5 eV below $E_F+\hbar\omega$ (25 eV above E_F). This peak broadens asymmetrically to lower energy with increasing exposure. At 1 ML exposure a second peak (labeled C' in Fig. 8) emerges at about 1.4 eV below $E_F+\hbar\omega$ (1.6 eV above E_F).

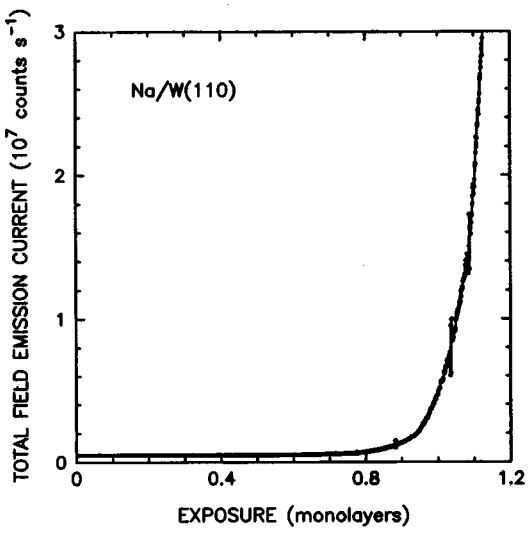

FIG. 6. Total field-emission current from the center of the W(110) facet at 300 K as a function of sodium exposure.

IV. DISCUSSION

A. Field effects on Na/W(100)

In the present experiments it proved to be impossible to measure the sodium-induced change in the work function

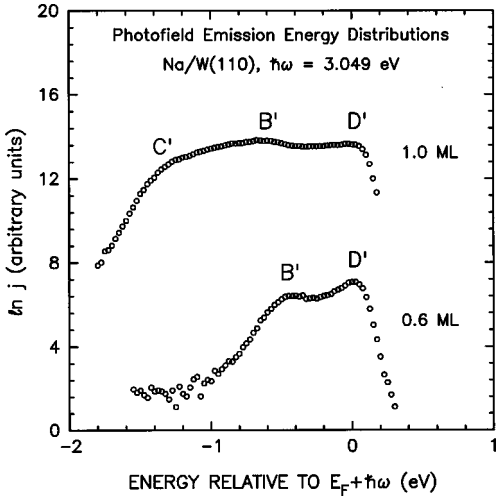

FIG. 8. Total-energy distributions for photofield emission at $\hbar\omega = 3.049$ eV from the (110) facet of tungsten at room temperature for sodium exposures of 0.6 ML (lower curve) and 1.0 ML (upper curve). The peaks labeled B' and C', and the shoulder D', are discussed in the text.

reliably, because at room temperature the sodium overlayer is strongly influenced by the applied electric field, resulting in irreproducible Fowler-Nordheim plots. Studies of Na/W(100) at 77 K have shown that the work function decreases rapidly with increasing sodium coverage, reaching a minimum at close to 1 ML.[14] Assuming that the coverage dependence of the work function at room temperature is similar to that at 77 K, the observed exposure dependence of the total-emission current below 1 ML is qualitatively consistent with the coverage dependence of the work function. In particular, the peak in the emission current near 1 ML is close to a minimum in the work function. The abrupt increase in emission observed above 1 ML exposure cannot, however, be attributed to work function changes.

While the field-emission pattern and the total-emission current depend strongly on the applied electric field, the shape of the total-energy distribution is essentially unchanged when the field is switched off and on again. Moreover, while a large transient increase in the emission current is observed whenever the applied electric field is switched off and on again, the emission current rapidly falls to its initial value. These observations are evidence that the electric field induces a reversible change in the configuration of the adatoms on the emitting facet. Neither field-enhanced tip contamination, nor field-induced desorption,[15] nor surface heating due to the field-emission current[16] is consistent with the data. However, a reversible field-induced rearrangement of sodium adsorbed on W(100) provides a consistent explanation for the present observations. Field-induced diffusion in adsorbate overlayers has been observed by other workers at field strengths comparable to those in the present experiments.[17–23] The present observations can be accounted for qualitatively in terms of field-induced changes in the adsorption energies of sodium on the various crystal planes of the tungsten field emitter.

B. Electronic structure Na/W(100)

A comparison between the total-energy distributions in field emission observed over a range of applied fields shows that the shape of the low-energy tail of the distribution does not depend on the total current passing through the probe hole. This rules out the possibility that the low-energy tail might be due to the inelastic scattering of electrons in the energy analyzer.[24] The low-energy and high-energy tails observed in field emission from W(100) in the presence of a monolayer of sodium imply that the sodium-enhanced emission is strongly energy dependent, and cannot be attributed solely to the effect of sodium in reducing the work function. The low-energy tail in field emission from Na/W(100) (labeled *A* in Fig. 3) is consistent with emission from a sodium-induced surface state or resonance on W(100) centered below the Fermi level.

The high-energy tails of the TEDs observed in field emission from Na/W(100) (labeled *B* and *C* in Fig. 3) are consistent with a broad sodium-induced surface state or resonance centered above E_F. This feature might also account for the low-energy tails of the photofield-emission distributions at an exposure of 1 ML (labeled *C* in Figs. 4 and 5). That the high-energy shoulders in the photofield-emission distributions (labeled *D* in Figs. 4 and 5) both occur at the same energy (3.2 eV above E_F) is a strong indication that they too are due to a feature of the electronic structure at the final-state energy.

C. Two-dimensional island formation on W(110)

Crystal growth studies identify three basic overlayer growth modes: three-dimensional crystalline growth on the bare substrate (Volmer-Weber mode), successive overlayer growth (Frank–van der Merwe mode), and three-dimensional crystallite growth on top of an intermediate overlayer (Stranski-Krastanov mode). Bauer and Poppa[25] have argued that the growth mode of an overlayer can be predicted from general thermodynamic considerations. The Volmer-Weber mode is expected if the free surface enthalpy of the adsorbate is greater than that of the substrate. When the surface energy of the adsorbate is lower than that of the substrate, the overlayer is expected to grow by the Frank–van der Merwe mode if its strain energy is small, while the Stranski-Krastanov mode is expected to dominate if the strain energy in the overlayer is large.

From the appearance of fluctuating bright spots in the field-emission pattern it is deduced that, above 1 ML exposure, sodium adsorbed at 300 K on the (110) facet of a tungsten field emitter forms a crystallitelike structure. The absence of bright spots in the field-emission pattern and of fluctuations in the tunneling current at less than 1 ML exposure suggests that the island grows on top of a homogeneous monolayer of sodium. Thus the present observations indicate that above 1 ML exposure of sodium on W(110) the overlayer grows according to the Stranski-Krastanov mode.

At low alkali-metal coverage, liquidlike phases are commonly observed in which the alkali-metal adatoms randomly occupy preferred adsorption sites. The adatoms are expected to aggregate to form islands when the adsorbate-adsorbate interaction is attractive and sufficiently strong compared with the interaction with the substrate. In the case of sodium adsorbed on tungsten, the predicted transfer of charge from the adsorbate to the substrate implies a strong electrostatic adsorbate-adsorbate repulsion. For this reason, island growth is not expected to occur in the first overlayer. In subsequent overlayers the ionic character of the adatoms is reduced because they are relatively weakly coupled to the substrate. In this case, it may become energetically favorable for the sodium atoms to aggregate to form islands or clusters. With varying coverage and temperature, the balance between the adsorbate-adsorbate interaction and the adsorbate-substrate interaction can yield a wide variety of ordered commensurate and incommensurate structures.[26] Incommensurate structures, in which densely packed atoms are forced out of high symmetry sites, are commonly formed after the completion of the first overlayer.

Low-energy electron diffraction (LEED) studies have shown that overlayers of sodium on W(100) grow pseudomorphically layer by layer up to 80 ML on W(100) in a centered (2×2) structure.[15] Each sodium atom is located at the center of a square formed by four tungsten atoms, resulting in an overlayer whose primitive translation vectors are rotated by 45° with respect to the tungsten [010] direction. The nearest-neighbor distance in each sodium overlayer is 4.47 Å, which is larger than the lattice constant of bulk sodium (4.29 Å). The field-emission pattern of Na/W(100),

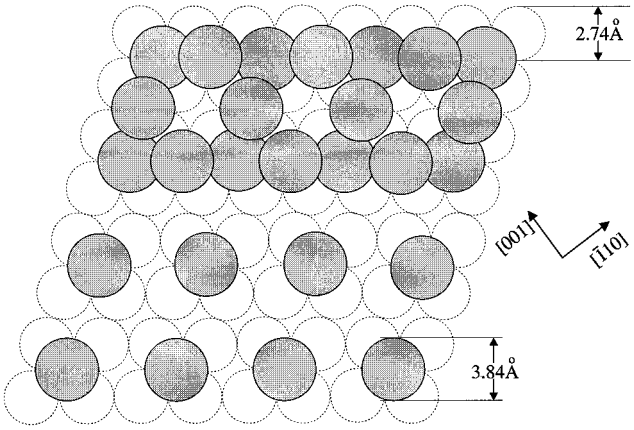

FIG. 9. Model structure for sodium adsorbed on the (110) facet of tungsten. The first overlayer assumes a (2×2) structure with a distance of 5.48 Å between the nearest neighbors. A more dense structure forms on top of the first overlayer.

which shows no evidence of island formation at any coverage, is consistent with successive overlayer growth.

The most likely arrangement for the sodium atoms in the first overlayer on the more densely packed W(110) plane is a simple (2×2) structure as shown in Fig. 9. The separation between the nearest-neighbor sodium atoms (5.48 Å) is quite large, as would be expected from the strong Coulomb repulsion. Above 1 ML, the adsorbate-adsorbate repulsion decreases and the sodium adatoms can aggregate on top of the first overlayer to form a planar island. However, while they achieve this configuration in the center of the (110) plane, sodium atoms near the edge are weakly bound to the island and can migrate to the surrounding high-index facets, resulting in an island whose size is governed largely by that of the facet. This picture is consistent with the observation that when the sodium exposure exceeds 1 ML the island that forms on the W(110) plane is apparently planar and of constant size.

D. Electronic structure of Na/W(110)

In contrast to Na/W(100), the TEDs in field emission from Na/W(110) (Fig. 7) show no indication of adsorbate-enhanced emission from below the Fermi level. In the photofield-emission spectra at 3.049 eV (Fig. 8), two distinct peaks are observed at 1.0 ML exposure; a weak shoulder (labeled C') about 1.6 eV above E_F and a broad peak (labeled B') about 2.5 eV above E_F. The absence of any corresponding initial-state structures in the field-emission spectra is a strong indication that they both correspond to structures in the surface density of states at the final-state energy.

E. Comparison between Na/W(100) and Na/W(110)

The photofield-emission data for Na/W(100) and Na/W(110) are very similar. At an exposure of 0.6 ML of sodium a broad peak in the surface density of states is observed, centered 2.2 eV above E_F on (100) (B in Fig. 5) and centered 2.5 eV above E_F on (110) (B' in Fig. 8). By 1.0 ML exposure the photofield-emission data show a region of strongly enhanced surface density of states extending from 1.4 to 3.0 eV above E_F on (100) (C to D in Fig. 5), and from 1.6 to 3.1 eV above E_F on (110) (C' to D'). By 1 ML the peak B cannot be detected on (100) but B' can still be detected on (100). In addition, the field-emission data provide evidence for strong adsorbate-induced emission from below E_F on (100), but not on (110).

The energy of each resonance is slightly lower on W(100) than on W(110). These differences in energy can be accounted for in terms of the comparative strength of the adsorbate-substrate interaction. On the more open (100) facet the sodium adatoms are in closer contact with the substrate than on the more densely packed (100) facet. The stronger adsorbate-substrate interaction on (100) would be expected to result in a greater lowering of the energies of the resonances.

Apart from the slight difference in their energies, the sodium-induced resonances observed on W(100) and W(110) are remarkably similar considering that the substrates are very different. This finding is an indication that the sodium-induced resonances observed in the surface densities of states are only weakly perturbed by interaction with the substrate. To date, all published calculations for submonolayer coverage and for singly adsorbed atoms are based on the jellium model, which is a useful guide to the physical situation provided that the electronic structure of the substrate does not play an important role. As one of the motivating factors for the present work is to establish an experimental basis to test methods for calculating the electronic structures of interfaces, it is instructive to compare the experimental data with the results of the jellium calculations.

For a singly adsorbed sodium atom, Lang[27] found that a significant fraction of the Na-3s charge is transferred to the substrate. The resonance that corresponds to the 3s valence level of the free atom is centered about 1.5 eV above the Fermi level. However, the 3s resonance is broadened by interaction with the jellium substrate, and an appreciable tail of this resonance remains below the Fermi level. Ishida[28] found that the 3s and the 3p_z components admix strongly, and concluded that the broad sodium-induced resonance about 1.5 eV above E_F involves the strongly hybridized states of Na-3s and Na-3p_z symmetry rather than pure Na-3s states. The final-state structure derived from the Na-3p_x and Na-3p_y atomic levels is expected to be both higher in energy and also narrower, as the 3p_x and 3p_y states are largely confined to the plane of the surface and interact only weakly with the electronic states of the substrate.

Most of the present experimental observations are consistent with the predictions of the jellium model. At low coverage, adsorbed sodium is expected to transfer a sizable fraction of the valence charge to the substrate. The resulting dipole layer at the interface decreases the work function, enhancing emission over the whole energy range, in agreement with the field-emission data. A comparison with the jellium calculations suggests that the final-state resonance (B,B') that is observed in the present experiments about 1.6 eV above E_F is derived from the Na-3p_x and Na-3p_y atomic levels, while the broad region of enhanced surface density of states (C-D,C'-D') is attributable to the 3s-3p_z resonance. However, while the features observed in the experimental TEDs are generally consistent with the low-lying electronic

levels of atomic sodium weakly perturbed by interaction with the substrate, the jellium model does not readily account for the sodium-enhanced field emission from below the Fermi level that is observed on W(100) but not on W(110).

No other studies of Na/W are available for comparison. However, Heskett, Frank, and Koch[29] have investigated the electronic structures of the alkali metals (Cs, K, Na) on Al(111) using inverse emission spectroscopy and ultraviolet photoemission spectroscopy. They interpreted their data in terms of unoccupied *np* resonances that shift to lower energy with increasing alkali-metal coverage. Simultaneously, the corresponding *ns* resonances were observed to shift to lower energy and to cross E_F. Their results are similar to the present observations.

V. CONCLUSIONS

The electronic structure of sodium adsorbed on the (100) and (110) facets of tungsten at room temperature has been studied by means of field- and photofield-emission spectroscopy. The field-emission patterns, the total-emission current, and the total-energy distributions have been measured as a function of exposure in the range from 0 to 1.2 ML. On the relatively open (100) facet of tungsten the adatom configuration is strongly influenced by the applied electric field. Above 1.2 ML exposure, the emission current proved to be not sufficiently stable to measure the total-energy distributions at 300 K. On the more densely packed (110) facet, an island is observed to grow on top of the first monolayer. The shape and size of the island are evidence of a planar character, but details of the structure are not known.

The sodium-induced structures observed in the surface densities of states on the (100) and (110) facets of tungsten are similar. A comparison with the results of jellium calculations suggests that they correspond to the $3s$-$3p_z$ and $3p_x$-$3p_y$ energy levels of sodium weakly perturbed by the interaction with the substrate. The small difference between the strengths of the substrate-adsorbate interaction on the two planes is attributed to the relatively large size of the sodium atom. That the substrate appears to play only a minor role justifies the application of the jellium model to describe the electronic structure of sodium adsorbed on tungsten. However, the jellium model does not readily account for the sodium-enhanced field emission from below the Fermi level that is observed on W(100) but not on W(110).

Work is currently under way to interpret the present results on the basis of self-consistent electronic structure calculations for the W(100) and W(110)-sodium-vacuum interfaces. The results of these calculations will be reported elsewhere. It would also be of interest to extend the present measurements to lower temperatures. This would give useful insights into the nature of the different adsorbate phases on tungsten, such as field-induced diffusion on W(100) and the conditions for island formation on W(110).

ACKNOWLEDGMENTS

We are grateful to Dr. G. A. Gaudin for his help and for many fruitful discussions, and to Dr. J. C. Chow for help with the preparation of the manuscript. This work was supported in part by operating and equipment grants from the Natural Science and Engineering Research Council (NSERC) of Canada. One of us (A.D.) wishes to acknowledge partial financial support from the University of Toronto.

[1] R. D. Diehl and R. McGrath, Surf. Sci. Rep. **23**, 43 (1996).
[2] R. W. Gurney, Phys. Rev. **47**, 479 (1935).
[3] B. Woratschek, W. Sesselmann, J. Küppers, G. Ertl, and H. Haberland, Phys. Rev. Lett. **55**, 1231 (1985).
[4] J. Lee, C. Hanrahan, J. Arias, F. Bozso, R. M. Martin, and H. Metiu, Phys. Rev. Lett. **54**, 1440 (1985).
[5] G. A. Gaudin and M. J. G. Lee, Surf. Sci. **280**, 91 (1993); **310**, 34 (1994); Phys. Rev. B **49**, 5575 (1994); G. A. Gaudin, Ph.D. thesis, University of Toronto, Toronto, 1993.
[6] E. Bauer, H. Poppa, G. Todd, and P. R. Davis, J. Appl. Phys. **48**, 3773 (1977).
[7] D. Venus and M. J. G. Lee, Surf. Sci. **125**, 452 (1983); **172**, 477 (1986).
[8] R. H. Good and E. W. Müller, in *Electron Emission*, edited by S. Flügge, Handbüch der Physik Vol. 21 (Springer, Berlin, 1956).
[9] R. D. Young and C. E. Kuyatt, Rev. Sci. Instrum. **39**, 1477 (1968).
[10] A. Modinos, *Field Emission, and Secondary Electron Emission Spectroscopy* (Plenum, New York, 1984).
[11] H. Q. Nguyen, P. H. Cutler, T. E. Feuchtwang, N. Miscovsky, and A. A. Lucas, Surf. Sci. **160**, 331 (1985).
[12] C. Schwartz and M. W. Cole, Surf. Sci. **115**, 290 (1982).
[13] G. Gaudin and M. J. G. Lee, Surf. Sci. **185**, 283 (1987), and references therein.
[14] E. V. Klimenko and V. K. Medvedev, Fiz. Tverd. Tela (Leningrad) **10**, 1986 (1968) [Sov. Phys. Solid State **10**, 1562 (1969)].
[15] A. Mlynczak and R. Niedermayer, Thin Solid Films **28**, 37 (1974).
[16] L. W. Swanson, L. C. Crouser, and F. M. Charbonier, Phys. Rev. **151**, 327 (1966).
[17] H. Utsugi and R. Gomer, J. Chem. Phys. **37**, 1706 (1962).
[18] V. M. Gavrilyuk and A. G. Naumovets, Fiz. Tverd. Tela (Leningrad) **5**, 2792 (1963) [Sov. Phys. Solid State **5**, 2043 (1964)].
[19] L. D. Schmidt, J. Chem. Phys. **46**, 3830 (1967).
[20] R. Lewis and R. Gomer, Surf. Sci. **17**, 333 (1969).
[21] G. G. Vladimirov, B. K. Medvedev, and J. J. Sokolskaya, Fiz. Tverd. Tela (Leningrad) **12**, 539 (1970); [Sov. Phys. Solid State **12**, 413 (1970)].
[22] G. Greiner and D. Menzel, Surf. Sci. **84**, 129 (1979).
[23] M. Domke, J. H. Block, and M. Drechsler, Surf. Sci. **51**, 451 (1975).
[24] C. Lea and R. Gomer, Phys. Rev. Lett. **12**, 804 (1970).
[25] E. Bauer and H. Poppa, Thin Solid Films **12**, 167 (1972).
[26] H. P. Bonzel, A. M. Bradshaw, and G. Ertl, *Physics and Chemistry of Alkali Metal Adsorption* (Elsevier, Amsterdam, 1989); A. Zangwill, *Physics at Surfaces* (Cambridge University Press, Cambridge, England, 1984).
[27] N. D. Lang, Phys. Rev. Lett. **55**, 230 (1985).
[28] H. Ishida, Phys. Rev. B **38**, 8006 (1988).
[29] D. Heskett, K.-H. Frank, and E. E. Koch, Phys. Rev. B **36**, 1276 (1987).